



Contents lists available at ScienceDirect

Spectrochimica Acta Part A: Molecular and Biomolecular Spectroscopy

journal homepage: www.elsevier.com/locate/saa

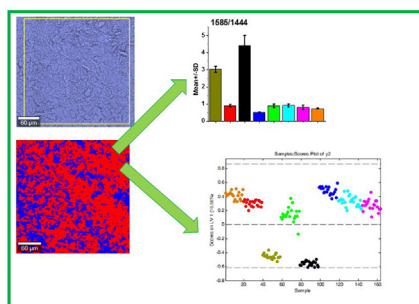
Raman imaging and statistical methods for analysis various type of human brain tumors and breast cancers

M. Kopec^{a,*}, M. Błaszczuk^b, M. Radek^b, H. Abramczyk^a^a Lodz University of Technology, Institute of Applied Radiation Chemistry, Laboratory of Laser Molecular Spectroscopy, Wroblewskiego 15, 93-590 Lodz, Poland^b Medical University of Lodz, Department of Neurosurgery, Spine and Peripheral Nerve Surgery, University Hospital WAM-CSW, Zeromskiego 113, 91-647 Lodz, Poland

HIGHLIGHTS

- Raman imaging and statistical methods show high potential in cancer diagnostics.
- Bands characteristic for carotenoids and cytochrome c allows tracking brain tumors.
- Metabolism of proteins and fatty acids allows monitoring aggressiveness in brain tumors.
- The ratios 1585/1655, 1585/1444, 1520/1585, 1156/1585, 1004/1585 provide information on aggressiveness in brain tumors.

GRAPHICAL ABSTRACT



ARTICLE INFO

Article history:

Received 29 April 2021

Received in revised form 14 June 2021

Accepted 16 June 2021

Available online 18 June 2021

Keywords:

Raman spectroscopy

Raman imaging

Brain tumor

Breast cancer

Raman biomarkers

ABSTRACT

Spectroscopic methods provide information on the spatial localization of biochemical components based on the analysis of vibrational spectra. Raman spectroscopy and Raman imaging can be used to analyze various types of human brain tumors and breast cancers. The objective of this study is to evaluate the Raman biomarkers to distinguish tumor types by Raman spectroscopy and Raman imaging. We have demonstrated that bands characteristic for carotenoids (1156 cm^{-1} , 1520 cm^{-1}), proteins (1004 cm^{-1}), fatty acids (1444 cm^{-1} , 1655 cm^{-1}) and cytochrome (1585 cm^{-1}) can be used as universal biomarkers to assess aggressiveness of human brain tumors. The sensitivity and specificity obtained from PLS-DA have been over 73%. Only for gliosarcoma WHO IV the specificity is lower and takes equal 50%. The presented results confirm clinical potential of Raman spectroscopy in oncological diagnostics.

© 2021 The Author(s). Published by Elsevier B.V. This is an open access article under the CC BY-NC-ND license (<http://creativecommons.org/licenses/by-nc-nd/4.0/>).

1. Introduction

The nervous system tumors are one of the most common types of cancer in the world. [1] In this paper we analyzed various types of human brain tumor such as: gliosarcoma [2], meningothelioma, anaplastic oligodendroglioma [3], pituitary adenoma [4], neurofibroma, testicular cancer metastasis to the brain and breast cancer. [5]

According to WHO meningotheliomas (Meningioma meningotheleale) account for some 15–18% of all intracranial tumors. Meningotheliomas are the most frequent brain tumors in adults and they occur more often in female than in male. [6] When meningotheliomas are benign tumor they carry a good prognosis. Standard treatment for meningotheliomas is surgical resection. It is estimated that 80% of meningotheliomas are grade I (mildly malignant). [7] The main symptoms in patient with meningotheliomas are sensory and motor deficits or gait disturbance. [8]

Malignant glioma is the most common type of primary brain tumor. There are known three subtypes of gliomas such as: anaplastic astrocytoma (AA), anaplastic oligoastrocytoma (AOA),

* Corresponding author.

E-mail address: monika.kopec@p.lodz.pl (M. Kopec).

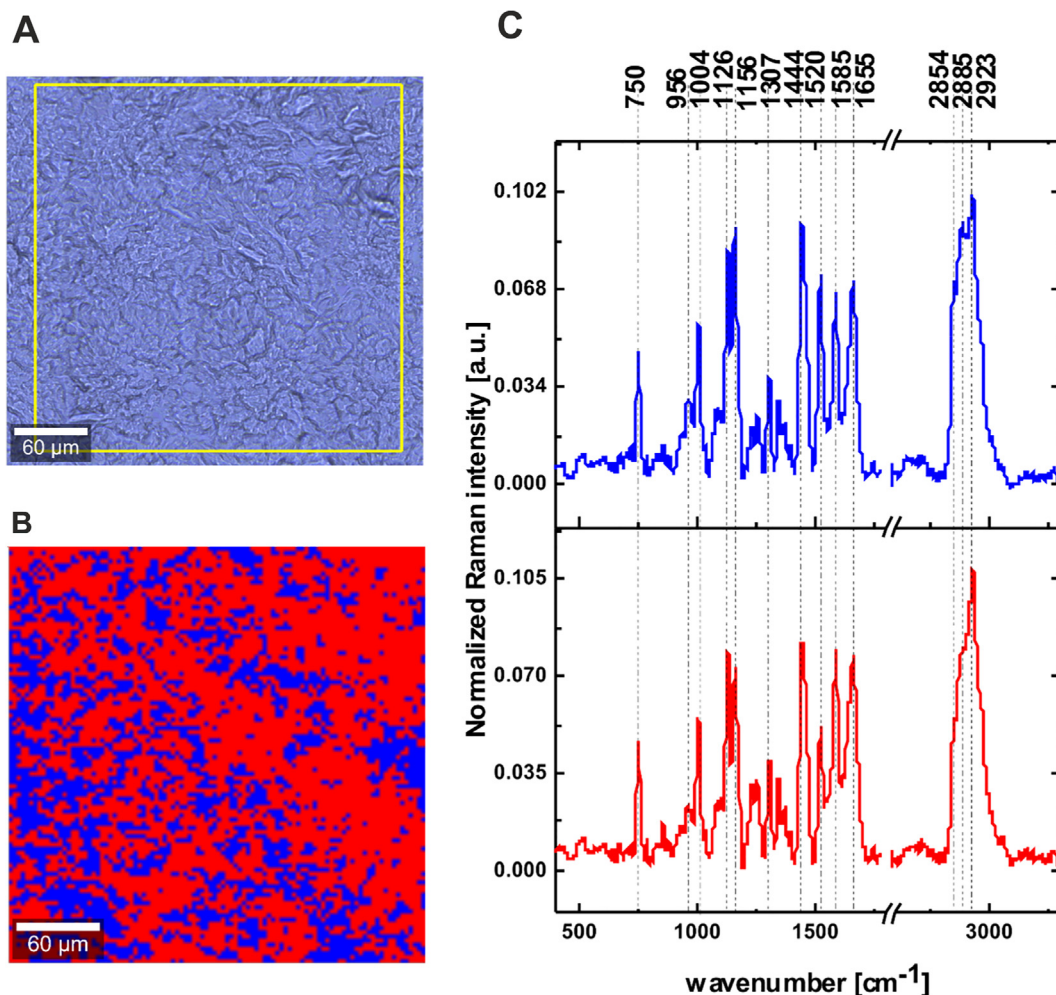


Fig. 1. Microscopy image (A), Raman image ($300 \mu\text{m} \times 300 \mu\text{m}$) constructed based on Cluster Analysis method, lipids (blue), proteins (red) (B) and Raman spectra (C) obtained by Cluster Analysis method in range $400\text{--}3300 \text{ cm}^{-1}$ from meningothelioma WHO grade I). Integration time for Raman images 0.5 s in the high frequency region and 1 s in the fingerprint region. The colours of the lines of the Raman spectra correspond to the colours of Raman image.

Table 1

The tentative assignments of Raman peaks [30,5,33,28,52,53].

Frequency [cm^{-1}]	Assignment
750	cytochrome
956	hydroxyproline/Collagen backbone
1004	proteins, phenylalanine
1126	cytochrome
1156	carotenoids
1228	nucleic acids (Try, Ala)/Proteins (Amide III β sheet or random coil), Lipid, phospholipid =C–H bend
1307	lipids, phospholipids
1444	CH_2 twist, collagen, protein amide III, DNA
1520	fatty acids, triglycerides, CH_2 or CH_3
1585	carotenoids
1655	cytochrome
2854	unsaturated fatty acids, triglycerides (C=C) str,
2885	lipids
2923	lipids, =CH str
3164	proteins str (NH), str (OH), amide, water

anaplastic oligodendroglioma (AO), and anaplastic ependymoma. Anaplastic oligodendroglioma tumors are rare and uncommon; they constitute 2–7% of primary brain tumors. [9] The standard therapy for patients with anaplastic oligodendroglioma and the

treatment include a lot of therapies such as: chemotherapy [10], stereotactic radiotherapies [11], targeted therapy [12], and reoperation. [13] Despite intensive study, the mortality among patients with malignant glioma is very high. It is estimated that 77% die within 1 year after diagnosis. [14]

A neurofibroma is a type of nerve tumor. Neurofibromas usually are benign peripheral nerve sheath usually single and commonly occur in all parts of the body. A neurofibroma may appear in people with a genetic disorder (neurofibromatosis type 1) or can arise with unknown cause. These nerve tumors most often occur in people of age 20–40 years. Neurofibromas look like little “rubber balls” under the skin. They can also protrude from the skin. [15] For the first time the neurofibroma was described by Von Recklinghausen in 1882. [16] The morbidity and mortality caused by neurofibromatosis depend on the occurrence of complications that involve any of the body system. [17]

Pituitary adenomas are tumors occurring in the anterior pituitary. Most pituitary tumors are benign and slow-growing. Pituitary adenoma can be classified as microadenoma, macroadenoma, and giant tumors depending on the tumor size. Tumors smaller than 10 mm are considered to be microadenomas, while macroadenomas are tumors larger than 10 mm. In contrast giant pituitary tumors are larger than 40 mm. [18] For patients with pituitary adenomas there are available treatment options such as: surgical excision, medical and radiation therapy. [18]

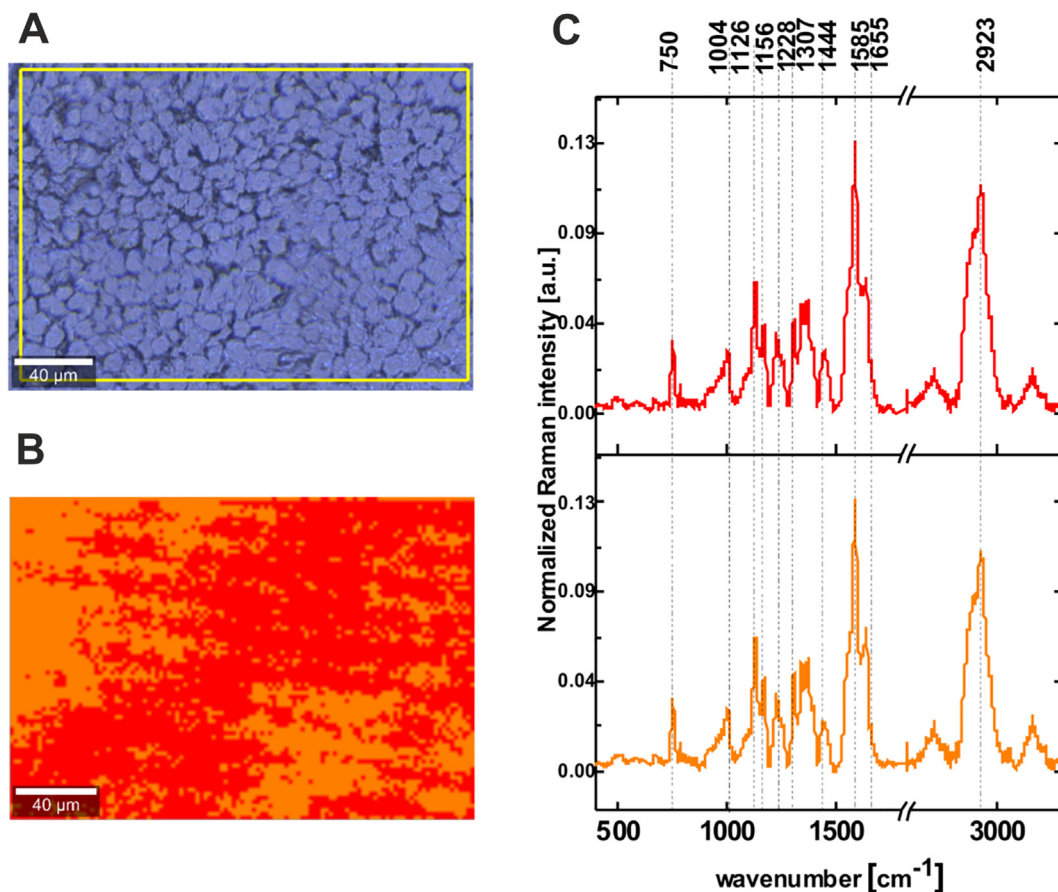


Fig. 2. Microscopy image (A), Raman image ($230\ \mu\text{m} \times 160\ \mu\text{m}$) constructed based on Cluster Analysis method, proteins (orange and red) (B) and Raman spectra (C) obtained by Cluster Analysis methods in range $400\text{--}3300\ \text{cm}^{-1}$ anaplastic oligodendroglioma WHO grade III). Integration time for Raman images 0.5 s in the high frequency region and 1 s in the fingerprint region. The line colours of the Raman spectra correspond to the colours of Raman image.

When cancer cells spread from their original site to the brain, metastases occur. The most likely types of cancer which spread to brain are: lung cancer, melanoma, colon cancer and breast cancer, less often testicular cancer. It is estimated that brain metastases occur in 10 to 30 percent of adults with diagnosed cancer. [19]

Surgery is the most common form of treatment for brain tumor.

For comparison, we studied also another type of cancers which belong to different class of phenotypes. According to WHO invasive ductal carcinoma (IDC) is one of the most common types of cancer among breast cancers. Invasive ductal carcinoma occurs more often in elderly woman but can affect women at any age [20,21].

One of the main reasons for insufficient progress in brain tumor and breast cancer diagnostics is related to the fact that most cancer types are not only heterogeneous in their genetic and biochemical composition but also reside in varying microenvironments and interact with different cell types. Until now, no technology has been fully proven for effective detecting of invasive cancer infiltrating the extracellular matrix. Nowadays cancer diagnostics is based on X-rays imaging, such as mammography and computer tomography, positron emission tomography, single photon emission computed tomography, magnetic resonance imaging, ultrasound imaging and histopathological analysis. None of these methods are effective in detecting invasive cancer infiltrating the extracellular matrix due to lack of information on biochemical composition, limited spectral or spatial resolution and limited specificity. [22,23,24]

So that, development of novel treatment strategies is needed. Raman spectroscopy and Raman imaging gives objective information on biochemical composition (chemical fingerprint), which is

not available from mentioned above techniques-biochemical information. Moreover Raman techniques have high spectral and spatial resolution. Tashibu presented first results obtained with the use of Raman spectroscopy in brain tumor analysis. [25] He analyzed the water content in brain tissues. This preliminary study gave impetus to further investigations. Several groups have used Raman spectroscopy to diagnosis brain tumors. Abramczyk et al showed the differences between tumor tissues and healthy tissues. [26,27,28,29,30] Byrne and colleagues in review presented the state of the art of Raman applications in the areas of *in vivo*, *ex vivo* and *in vitro*. [31] The most important achievements Orringer's group was application of stimulated Raman scattering during brain operation. [32] Another groups Gajjar with colleagues presented the capability to differentiate brain tumors and healthy brain tissue using Raman spectroscopy. [33] The potential of using Raman spectroscopy to analyses brain tumor was investigated also by Kirsch et al [34] and Krafft et al. [35]

The combination of Raman spectroscopy and Raman imaging offers information about location and distribution of chemical components inside cancers. Abramczyk et al in numerous papers have investigated the application of Raman spectroscopy and Raman imaging to diagnose infiltrating ductal carcinoma. [26,36,37,27,38,39,40,41] Look inside ductal carcinoma first reported by Abramczyk et al provided biochemical composition inside normal and cancerous human duct. It has been demonstrated that carotenoids, mammaglobin, palmitic acid and sphingomyelin are diagnostic biomarkers for breast cancer prognosis. [36] Another groups Alfano et al presented the capability to differentiate breast cancers and healthy breast tissue using Raman spectroscopy. [42] Stone et al in review presented the complementary

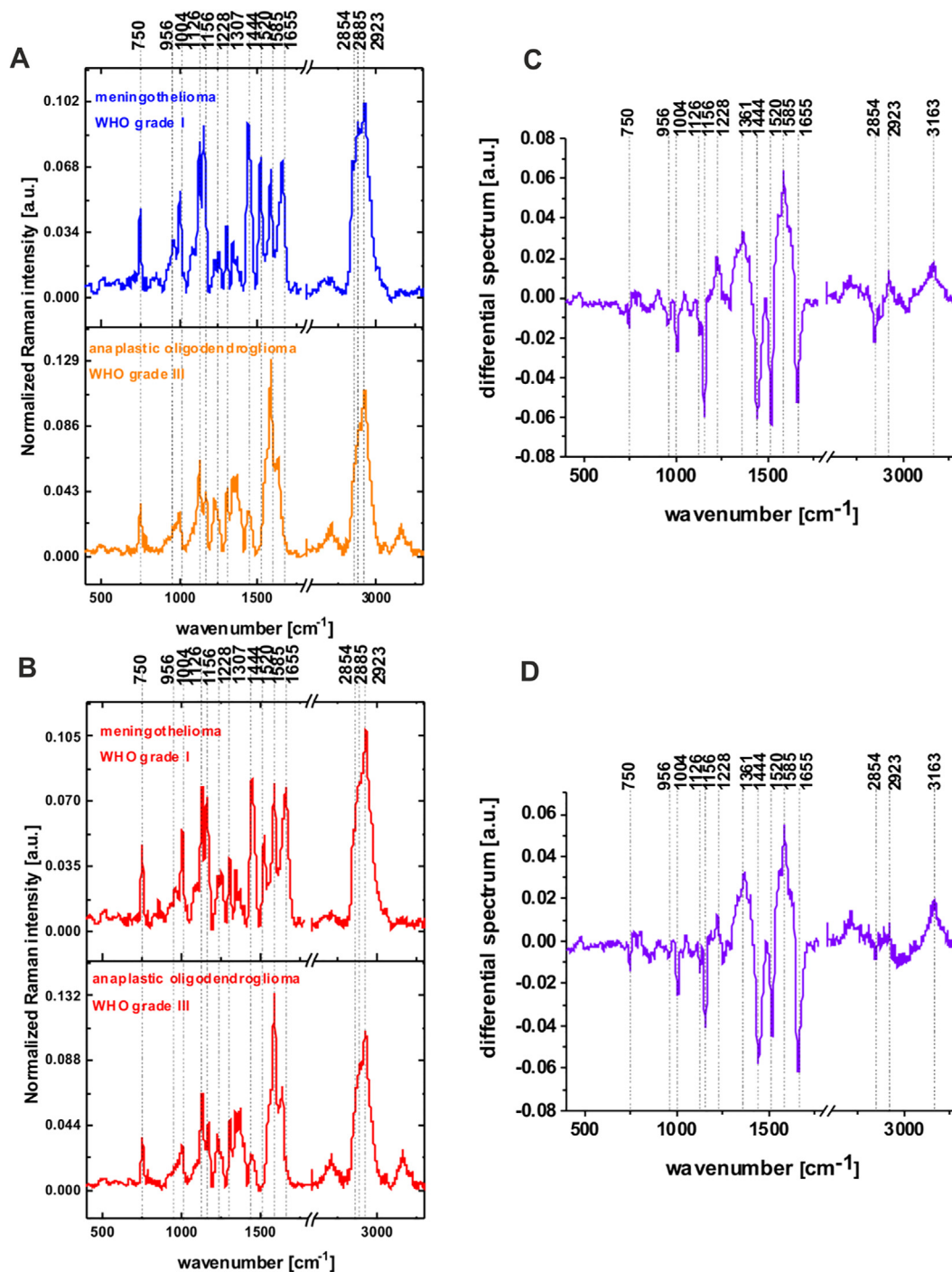


Fig. 3. Average Raman spectrum of meningioma WHO grade I (blue line for lipids, red line for proteins) and anaplastic oligodendroglioma WHO grade III (red and orange line for proteins) in the fingerprint region and in the high-frequency region (A,B); differential spectrum (malignant tumor–mildly malignant tumor) (purple line) in the fingerprint region and in the high-frequency region (C, D).

advantages of using Raman spectroscopy for cancer diagnostics [43,44].

Raman spectroscopy and Raman imaging made possible to monitor distribution of biochemical components in brain tumors and breast cancers. The components can be divided into subgroups such as: structural [45], metabolic [46], epigenetic [47], immunologic [48] and genetic [49].

In this paper we present Raman spectroscopy as a tool for distinguishing various subtypes of human brain tumor and breast cancer.

2. Materials and methods

2.1. Tissue preparation

The brain tissues were obtained from the material removed over the operation from Department of Neurosurgery, Spine and Peripheral Nerve Surgery, University Hospital WAM-CSW, Lodz. The breast tissue was obtained during routine surgery from the WWCoiT Nicolaus Copernicus in Lodz. Obtaining samples did not affect the course of the operation or treatment of the patients.

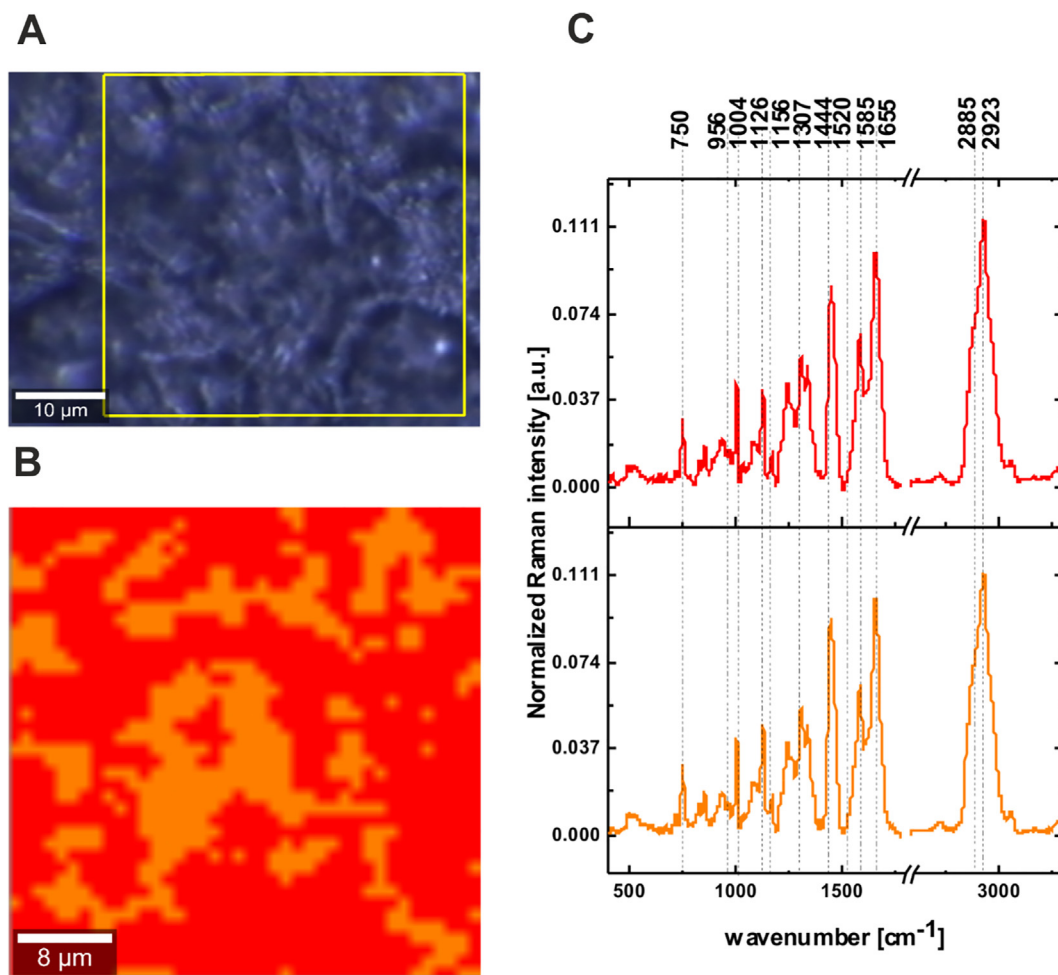


Fig. 4. Microscopy image (A), Raman image ($40\ \mu\text{m} \times 40\ \mu\text{m}$) constructed based on Cluster Analysis method, proteins (orange and red) (B) and Raman spectra (C) obtained by Cluster Analysis methods in range $400\text{--}3300\ \text{cm}^{-1}$ from invasive ductal carcinoma WHO III. Integration time for Raman images 0.5 s in the high frequency region and 0.5 s in the fingerprint region. The line colours of the Raman spectra correspond to the colours of Raman image.

The tissue brain and breast sections after cutting into $16\ \mu\text{m}$ thick slices in microtome were put on CaF_2 windows (Crystran). For all experiments we used only human fresh brain and breast tissue. We do not use the procedure formalin fixation, paraffin-embedding because of its influence on Raman measurements. [50] Written informed consent was obtained from patients. All experiments were conducted in accordance with relevant guidelines and regulations of the Bioethical Committee at the Medical University of Lodz, Poland (RNN/247/19/KE) and (RNN/323/17/KE/17/10/2017).

2.2. Raman spectroscopy, Raman imaging and statistical methods

All Raman spectra and Raman imaging presented in this manuscript were obtained using alpha 300 RSA+ (WITec, Germany) combined with confocal microscope coupled via the fibre of a 50 mm core diameter with an UHTS (Ultra High Throughput Spectrometer) spectrometer and a CCD Camera (Andor Newton DU970N-UVB-353) operating in standard mode with 1600×200 pixels at 60C with full vertical binning. All experiment were performed using laser beam (SHG of the Nd:YAG laser (532 nm)) and 40x dry objective (Nikon, objective type CFI Plan Fluor CELWD DIC-M, numerical aperture (NA) of 0.60 and a 3.6–2.8 mm working distance). All Raman experiments were performed using laser with a power 10 mW at the sample position. Every day before Raman measure-

ments the confocal system was calibrated using silicon plate ($520.7\ \text{cm}^{-1}$). Each Raman spectra and Raman imaging were processed to remove cosmic rays, smoothing (Savitzky-Golay method) and background subtraction. Preprocessing was performed using WITec Plus Software. Raman maps data were analysed using Cluster Analysis method. Detailed description of equipment and methodology used in the paper is available elsewhere [51,40,36].

The Raman spectra were obtained from 9 patients. Among patients with brain tumors 1 were diagnosed with testicular cancer metastasis, 1 with gliosarcoma WHO IV, 1 with anaplastic oligodendroglioma WHO III, 1 with meningioma WHO II, 1 with meningothelioma WHO I, 2 with pituitary adenoma and 1 with neurofibroma. Breast cancer sample was diagnosed with invasive ductal carcinoma WHO III. For each patient thousands of spectra from different sites of the sample were obtained from cluster analysis. In detail, for sample with testicular cancer metastasis we used typically 8400 Raman spectra for averaging, for sample with gliosarcoma WHO IV 6400 Raman spectra, for sample with anaplastic oligodendroglioma WHO III 9200 Raman spectra, for sample with meningioma WHO II 3000 Raman spectra, for sample with meningothelioma WHO I 90,000 Raman spectra, for 2 patients with pituitary adenoma 15,000 Raman spectra, for sample with neurofibroma 3600 Raman spectra and for the sample with invasive ductal carcinoma WHO III 1600 Raman spectra, respectively. Partial Least Squares Discriminant Analysis was performed using

Mathlab and PLS_Toolbox Version 4.0. Detailed description of chemometric methods was presented in our previous paper [38,51].

All results regarding the analysis of the intensity of the Raman spectra as a function of brain tumor or breast cancer grades are presented as the mean \pm SD, where p less than 0.05 (SD—standard deviation, p —probability value). Raman bands' intensity were taken and normalized by vector norm spectra. A significance level of less than 0.05 was used for all statistical analyses.

3. Results and discussion

The experiments were carried out using Raman spectroscopy and Raman imaging. Firstly, we focused on the Raman spectroscopy analysis for mildly malignant and malignant brain tumors.

Fig. 1 present the video image, Raman image and Raman spectra of the tissue of meningioma (Meningioma meningotheliale, WHO grade I). Raman images were performed by using Cluster Analysis method in the spectral region 400–3300 cm^{-1} .

Fig. 1 shows distribution of main components of mildly malignant tumor brain tissue in Raman image. One can see that the region is heterogeneous and is dominated by lipids (blue) and protein (red). In lipid rich region one can see a peak at 2854 cm^{-1} which is absent in protein rich region. Moreover peak at 1520 cm^{-1} corresponding to carotenoids is more visible in lipid rich region. From Fig. 1 one can see that spectra of mildly aggressive tumors are dominated by the peaks at 750, 956, 1004, 1126, 1156, 1307, 1444, 1520, 1585, 1655 cm^{-1} in the fingerprint region and by the peaks at 2854, 2885, 2923 cm^{-1} in the high frequency region. Detailed spectral informations for biochemical components assigned to the Raman vibrations are presented in Table 1.

To compare the biochemical composition of mildly malignant and highly aggressive brain tumors and we conducted the same analysis for malignant brain tissue (anaplastic oligodendroglioma WHO grade III). Fig. 2 presents the video image, Raman image and Raman spectra of the tumor brain tissue.

From Fig. 2 we can see that spectra of malignant human brain tumor are dominated by the peaks at 750, 1004, 1126, 1156, 1228, 1307, 1444, 1585, 1655 cm^{-1} in fingerprint region and by the peak at 2923 cm^{-1} in high frequency region. One can see from Fig. 2 that in contrast to mildly malignant tumors (Fig. 1) malignant brain tumor show high level of homogeneity. These vibrations correspond to protein rich region and we do not observe the peaks characteristic for the lipid rich ones. One can see that both clusters are almost identical and they differ only with intensity.

Detailed spectral information for biochemical components are presented in table 1 [30,33,5,53,28].

From Fig. 1 and Fig. 2 one can see that the main differences between the mildly malignant and malignant brain tumors occur at 1585 cm^{-1} corresponding to reduced cytochrome *c* (Fe^{+2}). [52]

In order to understand better the difference between mildly malignant and malignant brain tumors we compared the average Raman spectra, presented on Fig. 3. The average spectra results are based on thousands of spectra obtained from the Cluster analysis. To determine the significant difference between the mildly malignant and malignant tumor tissue we present the differential Raman spectrum (mildly malignant brain tissue subtracted from malignant brain tissue) in the fingerprint region and in the high-frequency region (Fig. 3C, D).

Comparing the spectra from Fig. 3A–D more detailed biochemical information about the changes in cancer development is obtained. One can see that main biochemical differences are observed in the fingerprint region. When we compare the region dominated by lipids (blue line) from mildly malignant tissue with

the region dominated by proteins (orange line) from malignant tissue (Fig. 3A) one can see differences. Firstly, in malignant tumor the Raman intensities of the bands at 1307, 1341, 1371 and 1585 cm^{-1} are higher than in mildly malignant. Secondly the bands at 750, 1004, 1126, 1156, 1444, 1655, 2854 and 2882 cm^{-1} are much stronger in mildly malignant brain tissue than in malignant ones (Fig. 3C). This observation confirms that mildly malignant tissue in contrary to the malignant one has higher concentration of lipids and fatty acid. In contracts, the malignant tissue contains more proteins. Comparing the region dominated by proteins (red line) from mildly malignant tissue and from malignant tissue (Fig. 3B) one can see also that the peaks at 1307, 1341, 1371 and 1585 cm^{-1} are stronger in malignant tissue. In contrary bands at 1004, 1156, 1444 cm^{-1} are much stronger in mildly malignant brain tissue. In high frequency region we do not observed peaks at 2854 cm^{-1} (Fig. 3D). We can see that the most prominent changes that occur due to the development of cancer are connected with the peak 1585 cm^{-1} assigned to the vibration of heme group of cytochrome *c*. [52] The Raman intensity (and concentration) of reduced cytochrome *c* increases with brain tumor

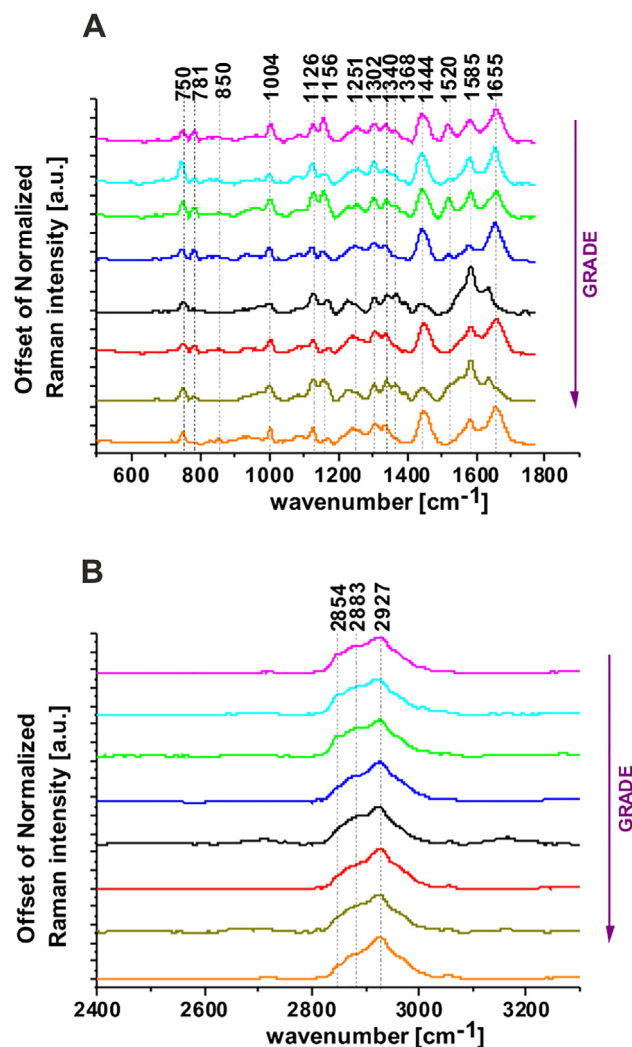


Fig. 5. The Raman spectra of the invasive ductal carcinoma WHO III (orange), testicular cancer metastasis (olive), gliosarcoma WHO IV (red), anaplastic oligodendroglioma WHO III (black), meningioma WHO II (blue), meningioma WHO I (green), pituitary adenoma (turquoise) and neurofibroma (magenta) in the fingerprint (A) and high frequency region (B).

aggressiveness. The previous studies reported similar observations. [52]

Spectacular difference is also observed at 1444 cm^{-1} . This band attributed to the lipids and fatty acids is much stronger in the mildly malignant tissue. Our results show higher lipid content in tumors of lower grade of malignancy. Previous studies reported similar observations [51,28,54].

Bands at 1156 and 1520 cm^{-1} corresponding to carotenoids are clearly observed in the mildly malignant tissue in contrast to the malignant tissue. The band associated to unsaturated fatty acids at 1655 cm^{-1} is higher in mildly malignant tissue than in malignant tissue. The role of carotenoids and unsaturated fatty acids was discussed of our previous papers [36,26,41].

Motivated by our recent research that suggest abnormal lipid metabolism for various cancers [51,55,54] and the results presented so far in this paper for brain tumors we wanted to check if this finding is more universal cancer hallmark for another types of phenotypes.

The correlation between lipid metabolism and cancer invasiveness is further explored in breast cancer. To test biochemical composition of human breast tissue we performed the same Raman procedure as for brain for invasive ductal carcinoma WHO III. Fig. 4 presents the video image, Raman image and Raman spectra of the cancerous human breast tissue.

One can see from Fig. 4 that the cancerous breast tissue is dominated peaks $750, 956, 1004, 1126, 1307, 1444, 1585, 1655, 2885$ and 2923 cm^{-1} . We do not observe Raman peaks at 1156 and 1520 cm^{-1} attributed to carotenoids that are clearly visible in mildly malignant tumor (Fig. 1).

From Figs. 2 and 4 which present malignant brain tumor (anaplastic oligodendroglioma WHO grade III) and malignant breast cancer (invasive ductal carcinoma WHO III) one can see that the both clusters (red and orange) in both types of malignancy are almost identical and different only with intensity. Both the malignant brain tumor and malignant breast cancer show high level of homogeneity with absence of lipid regions.

To understand in more details the biochemical changes that occur in tumors we measured and analyzed the Raman spectra in various types of human brain tumors and compared with breast cancer. Fig. 5 shows the Raman spectra of the brain tumor tissue (testicular cancer metastasis, gliosarcoma WHO IV, anaplastic oligodendroglioma WHO III, meningioma WHO II, meningothelioma WHO I, pituitary adenoma, neurofibroma and invasive ductal carcinoma WHO III) in the fingerprint (A) and high frequency region (B).

Many significant biochemical differences between the various types of brain tumor can be observed. The most relevant differences presented on Fig. 5 are related to the vibrations of carotenoids ($1156\text{ cm}^{-1}, 1520\text{ cm}^{-1}$), fatty acids ($1444\text{ cm}^{-1}, 1655\text{ cm}^{-1}$), proteins (1004 cm^{-1}) and cytochrome (1585 cm^{-1}). First we observe that the band 1444 cm^{-1} assigned to fatty acids

is much stronger in all mildly malignant cancers. In contrast the band at 1585 cm^{-1} is much stronger in more aggressive brain tumor tissues. This band has a lower intensity in the mildly malignant brain tissue, indicating that the reduced cytochrome *c* concentration is much lower in the mildly malignant human brain tumor tissue than in the malignant tissue. Moreover, the bands of carotenoids (1156 cm^{-1} and 1520 cm^{-1}) are more visible in mildly malignant brain tumors. The band at 1655 cm^{-1} corresponding to fatty acids has higher intensity in the mildly malignant brain tumor tissue. From high frequency region (Fig. 5B) one can see that the band at 2854 cm^{-1} assigned to lipids show higher lipid content in mildly malignant human brain tumor tissue.

To access the diagnostic potential of Raman spectroscopy we calculated the Raman intensity ratios for characteristic Raman vibrations that can be useful in a stratification of malignancy for various cancers.

Table 2 and Fig. 6 illustrate the intensity and standard deviation for the ratios $1585/1655, 1585/1444, 1520/1585, 1156/1585, 1004/1585$. The presented results are based on Raman average spectra for each patient obtained during Raman imaging. The one-way ANOVA using the Tukey test was used to calculate the value significance, asterix * denotes that the differences are statistically significant, *p* Values ≤ 0.05 were accepted as statistically significant.

One can see from Fig. 6 and Table 2 that presented above ratios are useful to discriminate the type of human brain tumor. Analyzing the ratios for vibrations of lipids and proteins non-negligible differences are visible for the less aggressive brain tumor in comparison to the malignant brain tumor. The ratios $1585/1655$ and $1585/1444$ are significantly higher for malignant brain tumor tissue (testicular cancer metastasis, anaplastic oligodendroglioma WHO III). While for less aggressive human brain tissue (meningothelioma WHO I, meningioma WHO II, pituitary adenoma and neurofibroma) the ratios of $1520/1585, 1156/1585$ and $1004/1585$ are higher. All values of ratio presented on Fig. 6 for invasive breast carcinoma WHO III are comparable to the ratios for the gliosarcoma WHO IV. The observed discrimination between the various types of human brain tumor and breast cancer is based on Raman intensity ratios.

To better visualize the differences between various human brain tumors and human breast cancer we used chemometric analysis by statistical analysis using PLS-DA methods.

Fig. 7 shows the PLS-DA score plot for the Raman spectra of human brain and breast cancers. Fig. 7 shows evidently that differences between the cancer subtypes can be revealed.

The plots presented on Fig. 7 confirm the differences between human brain and breast cancers. The differences and similarities are visible by grouping the results into separate clusters. Moreover, Raman spectra for the most aggressive brain tumor (anaplastic oligodendroglioma WHO III (black colour) and testicular cancer metastasis (olive colour)) are the most separated from the rest of

Table 2

Raman intensity ratios, $1585/1655, 1585/1444, 1520/1585, 1156/1585, 1004/1585$ for, testicular cancer metastasis, gliosarcoma WHO IV, anaplastic oligodendroglioma WHO III, meningioma WHO II, meningothelioma WHO I, pituitary adenoma, neurofibroma, invasive ductal carcinoma WHO III, SD – standard deviation.

ratio	Testicular cancer metastasis	gliosarcoma WHO IV	Anaplastic Oligodendroglioma WHO III	meningioma WHO II	meningothelioma WHO I	Pituitary adenoma	Neurofibroma	Invasive ductal carcinoma WHO III
	Mean \pm SD	Mean \pm SD	Mean \pm SD	Mean \pm SD	Mean \pm SD	Mean \pm SD	Mean \pm SD	Mean \pm SD
1585/1655	2.8 ± 0.11	0.8 ± 0.06	4.95 ± 0.89	0.44 ± 0.02	1.02 ± 0.09	0.76 ± 0.06	0.7 ± 0.08	0.65 ± 0.02
1585/1444	3.04 ± 0.18	0.9 ± 0.07	4.43 ± 0.57	0.52 ± 0.02	0.9 ± 0.11	0.92 ± 0.09	0.81 ± 0.14	0.74 ± 0.03
1520/1585	0.37 ± 0.09	0.04 ± 0.01	0.1 ± 0.04	0.46 ± 0.04	0.8 ± 0.19	0.26 ± 0.18	0.87 ± 0.08	0.05 ± 0.02
1156/1585	0.54 ± 0.12	0.12 ± 0.02	0.34 ± 0.03	0.7 ± 0.13	1.12 ± 0.27	0.45 ± 0.1	1.12 ± 0.14	0.14 ± 0.006
1004/1585	0.4 ± 0.06	0.63 ± 0.08	0.25 ± 0.01	1.05 ± 0.08	0.84 ± 0.14	0.46 ± 0.05	0.94 ± 0.13	0.67 ± 0.03

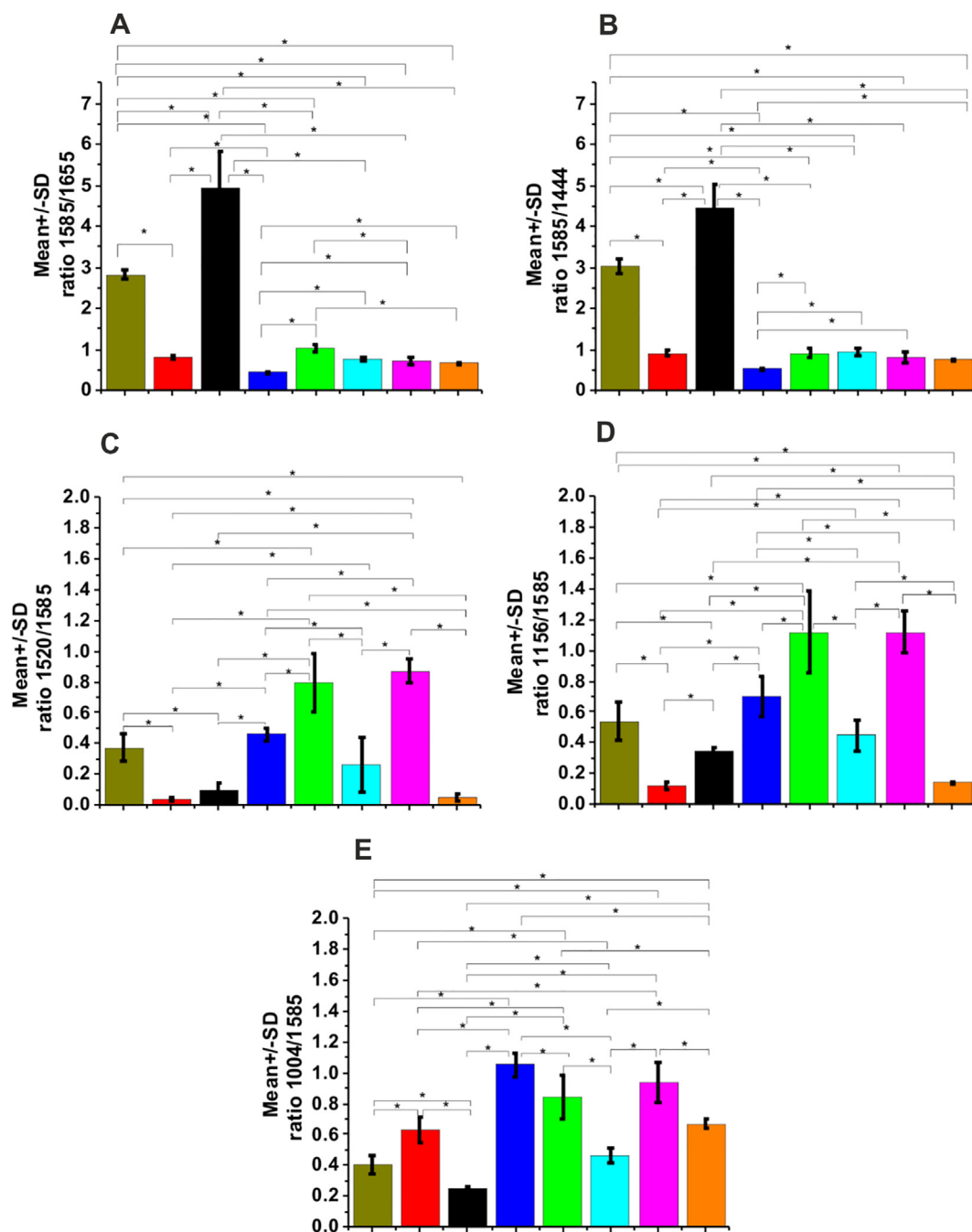


Fig. 6. The intensity ratios and SD for 1585/1655 (A), 1585/1444 (B), 1520/1585 (C), 1156/1585(D), 1004/1585 (E) for testicular cancer metastasis (olive), gliosarcoma WHO IV (red), anaplastic oligodendroglioma WHO III (black), meningioma WHO II (blue), meningothelioma WHO I (green), pituitary adenoma (turquoise), neurofibroma (magenta), invasive ductal carcinoma WHO III (orange). The statistically significant results have been marked with an asterix.

cancer subtypes. One can see that the Raman spectra for the most aggressive brain tumor (gliosarcoma WHO IV (red colour)) are mixed with Raman spectra for the aggressive breast cancer WHO III (orange colour). This result was presented also on Fig. 6 and Table 2.

To access the diagnostic potential of Raman spectroscopy and imaging for clinical practice we calculated sensitivity and specificity. Table 3 presents the value of sensitivity and specificity obtained from PLS-DA method. The high values for sensitivity and specificity highlight the importance of Raman spectroscopy and imaging as a new diagnostic tool.

4. Conclusions

In this exploratory study, we demonstrated that Raman spectroscopy, Raman imaging and statistical analysis are useful tools for human cancer diagnostics. For human brain tumor distinguishing vibrational signatures were primarily responsible for alterations in carotenoids, proteins, fatty acids and cytochrome *c*. Presented research suggest that Raman biomarkers in the future can provide additional insight into the biology of various types of human brain tumor and breast cancer. We have shown that bands characteristic for carotenoids, proteins, fatty acids and cytochrome

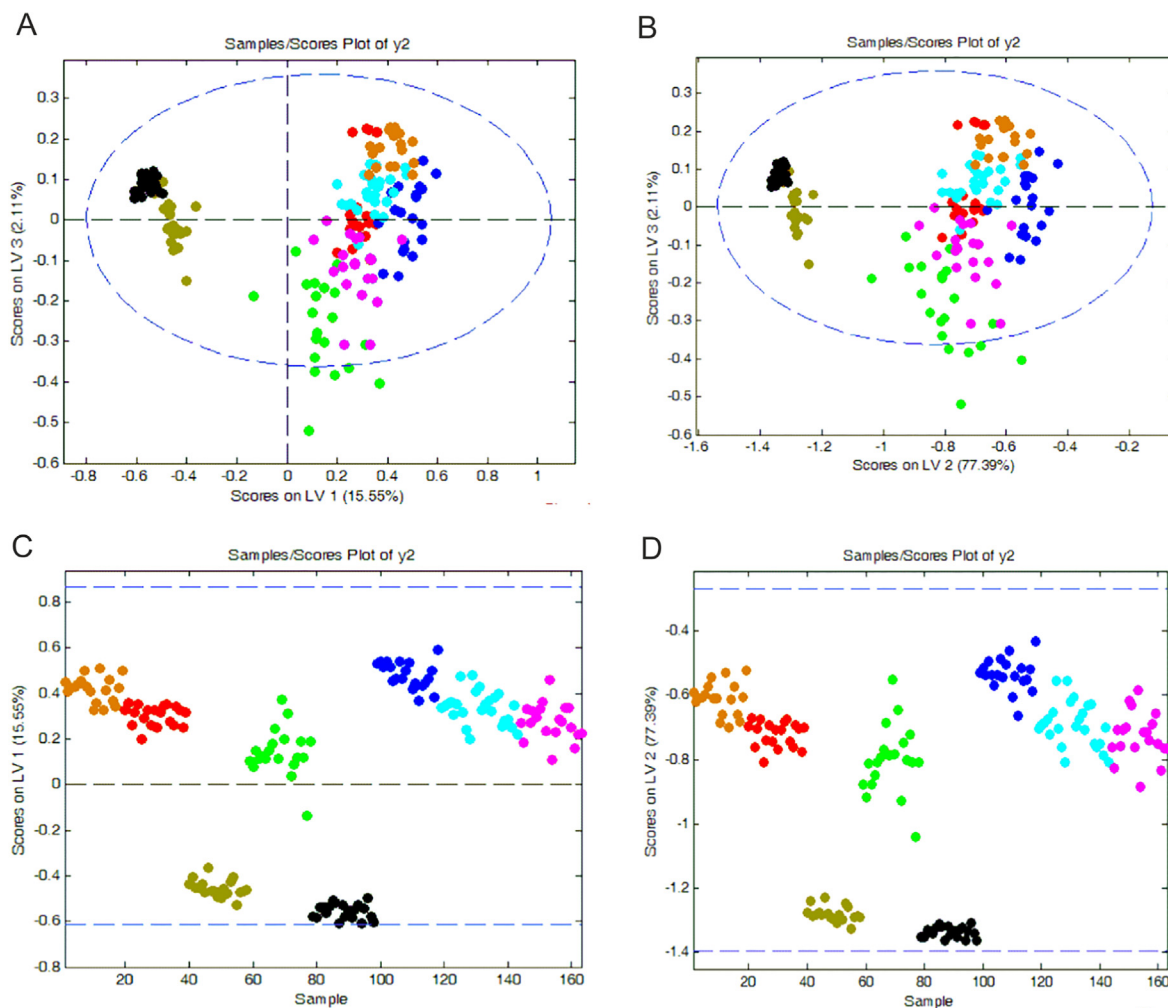


Fig. 7. PLS-DA score plot for the average Raman spectra for: Testicular cancer metastasis (olive), gliosarcoma WHO IV (red), anaplastic oligodendroglioma WHO III (black), meningioma WHO II (blue), meningothelioma WHO I (green), pituitary adenoma (turquoise), neurofibroma (magenta), invasive ductal carcinoma WHO III (orange).

Table 3

The value of sensitivity and specificity for calibration and cross validation procedure from PLS-DA analysis.

	Testicular cancer metastasis	gliosarcoma WHO IV	Anaplastic Oligodendroglioma WHO III	meningioma WHO II	meningothelioma WHO I	Pituitary adenoma	Neurofibroma	Invasive ductal carcinoma WHO III
Sensitivity (calibration)	0.947	0.950	1.0	1.0	0.900	0.960	0.900	0.947
Specificity (calibration)	0.861	0.497	0.986	0.797	0.916	0.616	0.741	0.896
Sensitivity (cross validation)	0.947	0.950	1.0	0.900	0.900	0.960	0.900	0.947
Specificity (cross validation)	0.861	0.497	0.986	0.804	0.916	0.623	0.727	0.903

c are changed in various brain tumors and breast cancer. The ratios 1585/1655, 1585/1444, 1520/1585, 1156/1585, 1004/1585 can be used as Raman biomarkers for diagnosing human brain tumors and breast cancer. We have demonstrated that Raman spectroscopy combined with statistical analysis would be non-subjective technique used as a method alongside neuropathology for brain cancer diagnosis. Raman spectroscopy combined with Raman imaging can be a powerful method for detecting invasive ductal carcinoma.

CRedit authorship contribution statement

M. Kopec: Conceptualization, Funding acquisition, Investigation, Methodology, Writing - original draft, Writing - original draft.

M. Błaszczuk: Investigation, Methodology. **M. Radek:** Investigation, Methodology. **H. Abramczyk:** Conceptualization, Funding acquisition, Methodology.

Declaration of Competing Interest

The authors declare that they have no known competing financial interests or personal relationships that could have appeared to influence the work reported in this paper.

Acknowledgement

This work was supported by the National Science Centre of Poland (Narodowe Centrum Nauki, UMO-2019/33/B/ST4/01961) and Miniatura 4 (grant 2020/04/X/ST4/00325).

References

- [1] C. Hardwidge, S. Hettige, Tumours of the central nervous system, *Surgery*. 30 (2012) 155–161, <https://doi.org/10.1016/j.mpsur.2011.12.008>.
- [2] F.K. Lu, D. Calligaris, O.I. Olubiyi, I. Norton, W. Yang, S. Santagata, X.S. Xie, A.J. Golby, N.Y.R. Agar, Label-free neurosurgical pathology with stimulated Raman imaging, *Cancer Res.* 76 (2016) 3451–3462, <https://doi.org/10.1158/0008-5472.CAN-16-0270>.
- [3] M. Jermyn, J. Desroches, J. Mercier, K. St-Arnaud, M.-C. Guiot, F. Leblond, K. Petrecca, Raman spectroscopy detects distant invasive brain cancer cells centimeters beyond MRI capability in humans, *Biomed. Opt. Express*. 7 (2016) 5129, <https://doi.org/10.1364/boe.7.005129>.
- [4] D. Bovenkamp, A. Micko, J. Püls, F. Placzek, R. Höftberger, G. Vila, R. Leitgeb, W. Drexler, M. Andreana, S. Wolfsberge, A. Unterhuber, Line scan raman microspectroscopy for label-free diagnosis of human pituitary biopsies, *Molecules* 24 (2019) 1–15, <https://doi.org/10.3390/molecules24193577>.
- [5] L.M. Fullwood, G. Clemens, D. Griffiths, K. Ashton, T.P. Dawson, R.W. Lea, C. Davis, F. Bonnier, H.J. Byrne, M.J. Baker, Investigating the use of Raman and immersion Raman spectroscopy for spectral histopathology of metastatic brain cancer and primary sites of origin, *Anal. Methods* 6 (2014) 3948–3961, <https://doi.org/10.1039/c3ay42190b>.
- [6] S. Portet, R. Naoufal, G. Tachon, A. Simonneau, A. Chalant, A. Naar, S. Milin, B. Bataille, L. Karayan-Tapon, Histomolecular characterization of intracranial meningiomas developed in patients exposed to high-dose cyproterone acetate: an antiandrogen treatment, *Neuro-Oncology Adv.* 1 (2019) 1–12, <https://doi.org/10.1093/noon/1.1.1>.
- [7] D.N. Louis, A. Perry, G. Reifenberger, A. von Deimling, D. Figarella-Branger, W.K. Cavenee, H. Ohgaki, O.D. Wiestler, P. Kleihues, D.W. Ellison, The 2016 World Health Organization Classification of Tumors of the Central Nervous System: a summary, *Acta Neuropathol.* 131 (2016) 803–820, <https://doi.org/10.1007/s00401-016-1545-1>.
- [8] C.L.M. Morais, T. Lilo, K.M. Ashton, C. Davis, T.P. Dawson, N. Gurusinge, F.L. Martin, Determination of meningioma brain tumour grades using Raman microspectroscopy imaging, *Analyst*. 144 (2019) 7024–7031, <https://doi.org/10.1039/c9an01551e>.
- [9] V.K. Puduvali, M. Hashmi, L.D. McAllister, V.A. Levin, K.R. Hess, M. Prados, K.A. Jaecle, W.K.A. Yung, S.S. Buys, J.M. Bruner, J.J. Townsend, R. Davis, R. Sawaya, A.P. Kyritsis, Anaplastic oligodendrogliomas: Prognostic factors for tumor recurrence and survival, *Oncology*. 65 (2003) 259–266, <https://doi.org/10.1159/000074479>.
- [10] R. Stupp, W.P. Mason, M.J. Van Den Bent, M. Weller, B. Fisher, M.J.B. Taphoorn, K. Belanger, A.A. Brandes, C. Marosi, U. Bogdahn, J. Curschmann, R.C. Janzer, S. K. Ludwin, T. Gorlia, A. Allgeier, D. Lacombe, J.G. Cairncross, E. Eisenhauer, R.O. Mirimanoff, 2005STUPP rt + tmz, *N. Engl. J. Med.* 352 (2005) 987–996, www.nejm.org.
- [11] P. Mulvenna, M. Nankivell, R. Barton, C. Favre-Finn, P. Wilson, E. McColl, B. Moore, I. Brisbane, D. Ardron, T. Holt, S. Morgan, C. Lee, K. Waite, N. Bayman, C. Pugh, B. Sydes, R. Stephens, M.K. Parmar, R.E. Langley, Dexamethasone and supportive care with or without whole brain radiotherapy in treating patients with non-small cell lung cancer with brain metastases unsuitable for resection or stereotactic radiotherapy (QUARTZ): results from a phase 3, non-inferiority, *Lancet* 388 (2016) 2004–2014, [https://doi.org/10.1016/S0140-6736\(16\)30825-X](https://doi.org/10.1016/S0140-6736(16)30825-X).
- [12] T.R. Daniels, E. Bernabeu, J.A. Rodríguez, S. Patel, M. Kozman, D.A. Chiappetta, E. Holler, J.Y. Ljubimova, G. Helguera, M.L. Penichet, The transferrin receptor and the targeted delivery of therapeutic agents against cancer, *Biochim. Biophys. Acta - Gen. Subj.* 2012 (1820) 291–317, <https://doi.org/10.1016/j.bbagen.2011.07.016>.
- [13] M.C. Chamberlain, S. Johnston, Bevacizumab for recurrent alkylator-refractory anaplastic oligodendroglioma, *Cancer* 115 (2009) 1734–1743, <https://doi.org/10.1002/cncr.24179>.
- [14] Y. Zhou, C.-H. Liu, B. Wu, X. Yu, G. Cheng, K. Zhu, K. Wang, C. Zhang, M. Zhao, R. Zong, L. Zhang, L. Shi, R.R. Alfano, Optical biopsy identification and grading of gliomas using label-free visible resonance Raman spectroscopy, *J. Biomed. Opt.* 24 (2019) 1, <https://doi.org/10.1117/1.jbo.24.9.095001>.
- [15] J.R. Antonio, E.M. Goloni-Bertollo, L.A. Tridico, Neurofibromatosis: chronological history and current issues, *Anal. Brailleiros de Dermatologia* 1 (2013) 329–343, <https://doi.org/10.1590/abd1806-4841.20132125>.
- [16] B.J. Canale, D.J. Von, Recklinghausen disease of the nervous system, in: P.J. Vinken, G.W. Bruyn, (Eds.) *Handbook of clinical neurology*, vol. 14. Amsterdam: Holland Publishing Company; 1972. pp. 132–162.
- [17] K. Khosrotehrani, S. Bastuji-garin, J. Zeller, J. Revuz, P. Wolkenstein, Clinical Risk Factors for Mortality in Patients With Neurofibromatosis 1 (2003) 139
- [18] M.E. Molitch, Diagnosis and Treatment of Pituitary Adenomas, *JAMA* (2017) 6–11, <https://doi.org/10.1001/jama.2016.19699>.
- [19] A. Willett, J. Ben Wilkinson, C. Shah, M.P. Mehta, Management of solitary and multiple brain metastases from breast cancer, *Indian J. Med. Paediatr, Oncol.* 36 (2015) 87–93, <https://doi.org/10.4103/0971-5851.158835>.
- [20] S.L. Gordo, J.B. Falp, E. Lopez-gordo, E.J. Roig, J.E. Mendez, J.S. Calvo, Influence of ductal carcinoma in situ on the outcome of invasive breast cancer. A prospective cohort study, *Int. J. Surg.* 63 (2019) 98–106, <https://doi.org/10.1016/j.ijsu.2019.01.016>.
- [21] W. San-Gang, Z. Wen-Wen, S. Jia-Yuan, H. Zhen-Yu, Prognostic value of ductal carcinoma in situ component in invasive ductal carcinoma of the breast : a Surveillance, Epidemiology, and End Results database analysis, *Cancer Manag. Res.* (2018) 527–534, <https://doi.org/10.2147/CMAR.S154656>.
- [22] A. Raikhlin, B. Curpen, E. Warner, C. Betel, B. Wright, R. Jong, Breast MRI as an adjunct to mammography for breast cancer screening in high-risk patients: Retrospective review, *Am. J. Roentgenol.* 204 (2015) 889–897, <https://doi.org/10.2214/AJR.13.12264>.
- [23] N. Mori, N. Nakamura, K. Taniguchi, C. Hamaguchi, Magnetophonon Resonance at High Electric and Magnetic Fields in Small n+nn+ GaAs Structures, *J. Phys. Soc. Japan*. 57 (1988) 205–216, <https://doi.org/10.1143/JPSJ.57.205>.
- [24] K.Y. Sang, N. Cho, K.M. Woo, The role of PET/CT for evaluating breast cancer, *Korean J. Radiol.* 8 (2007) 429–437, <https://doi.org/10.3348/kjr.2007.8.5.429>.
- [25] K. Tashibu, Analysis of water content in rat brain using Raman spectroscopy, *No To Shinkei*. 42 (1990) 999–1004.
- [26] H. Abramczyk, A. Imiela, B. Brozek-Pluska, M. Kopec, Advances in Raman imaging combined with AFM and fluorescence microscopy are beneficial for oncology and cancer research, *Nanomedicine* 14 (2019) 1873–1888, <https://doi.org/10.2217/nmm-2018-0335>.
- [27] H. Abramczyk, B. Brozek-Pluska, A. Jarota, J. Surmacki, A. Imiela, M. Kopec, A look into the use of Raman spectroscopy for brain and breast cancer diagnostics: linear and non-linear optics in cancer research as a gateway to tumor cell identity, *Expert Rev. Mol. Diagn.* 20 (2020) 99–115, <https://doi.org/10.1080/14737159.2020.1724092>.
- [28] A. Imiela, B. Polis, L. Polis, H. Abramczyk, Novel strategies of Raman imaging for brain tumor research, *Oncotarget* 8 (2017) 85290–85310, <https://doi.org/10.18632/oncotarget.19668>.
- [29] M. Kopec, A. Imiela, H. Abramczyk, Monitoring glycosylation metabolism in brain and breast cancer by Raman imaging, *Sci. Rep.* (2019) 1–13, <https://doi.org/10.1038/s41598-018-36622-7>.
- [30] H. Abramczyk, A. Imiela, The biochemical, nanomechanical and chemometric signatures of brain cancer, *Spectrochim. Acta - Part A Mol. Biomol. Spectrosc.* 188 (2018) 8–19, <https://doi.org/10.1016/j.saa.2017.06.037>.
- [31] M.J. Baker, H.J. Byrne, J. Chalmers, P. Gardner, R. Goodacre, A. Henderson, S.G. Kazarian, F.L. Martin, J. Moger, N. Stone, J. Sulé-Suso, Clinical applications of infrared and Raman spectroscopy: State of play and future challenges, *Analyst* 143 (2018) 1735–1757, <https://doi.org/10.1039/c7an01871a>.
- [32] D.A. Orringer, B. Pandian, Y.S. Niknafs, T.C. Hollon, J. Boyle, S. Lewis, M. Garrard, S.L. Hervey-Jumper, H.J.L. Garton, C.O. Maher, J.A. Heth, O. Sagher, D.A. Wilkinson, M. Snuderl, S. Veneti, S.H. Ramkissoon, K.A. McFadden, A. Fisher-Hubbard, A.P. Lieberman, T.D. Johnson, X.S. Xie, J.K. Trautman, C.W. Freudiger, S. Camelo-Piragua, Rapid intraoperative histology of unprocessed surgical specimens via fibre-laser-based stimulated Raman scattering microscopy, *Nat. Biomed. Eng.* 1 (2017), <https://doi.org/10.1038/s41551-016-0027>.
- [33] K. Gajjar, L.D. Heppenstall, W. Pang, K.M. Ashton, J. Trevisan, I.I. Patel, V. Llabjani, H.F. Stringfellow, P.L. Martin-Hirsch, T. Dawson, F.L. Martin, Diagnostic segregation of human brain tumours using Fourier-transform infrared and/or Raman spectroscopy coupled with discriminant analysis, *Anal. Methods*. 5 (2013) 89–102, <https://doi.org/10.1039/c2ay25544h>.
- [34] M. Kirsch, G. Schackert, R. Salzer, C. Krafft, Raman spectroscopic imaging for in vivo detection of cerebral brain metastases, *Anal. Bioanal. Chem.* 398 (2010) 1707–1713, <https://doi.org/10.1007/s00216-010-4116-7>.
- [35] C. Krafft, B. Belay, N. Bergner, B.F.M. Romeike, R. Reichart, R. Kalf, J. Popp, Advances in optical biopsy-correlation of malignancy and cell density of primary brain tumors using Raman microspectroscopic imaging, *Analyst* 137 (2012) 5533–5537, <https://doi.org/10.1039/c2an36083g>.
- [36] H. Abramczyk, B. Brozek-Pluska, New look inside human breast ducts with Raman imaging. Raman candidates as diagnostic markers for breast cancer prognosis: Mammaglobin, palmitic acid and sphingomyelin, *Anal. Chim. Acta*. 909 (2016) 91–100, <https://doi.org/10.1016/j.aca.2015.12.038>.
- [37] H. Abramczyk, B. Brozek-Pluska, Apical-basal polarity of epithelial cells imaged by Raman microscopy and Raman imaging: Capabilities and challenges for cancer research, *J. Mol. Liq.* (2017), <https://doi.org/10.1016/j.jmolliq.2017.05.142>.
- [38] B. Brozek-Pluska, M. Kopec, H. Abramczyk, Development of a new diagnostic Raman method for monitoring epigenetic modifications in the cancer cells of human breast tissue, *Anal. Methods* 8 (2016) 8542–8553, <https://doi.org/10.1039/c6ay02559e>.
- [39] J. Surmacki, J. Musial, R. Kordek, H. Abramczyk, Raman imaging at biological interfaces: Applications in breast cancer diagnosis, *Mol. Cancer*. 12 (2013) 1–12, <https://doi.org/10.1186/1476-4598-12-48>.
- [40] M. Kopec, H. Abramczyk, Angiogenesis - a crucial step in breast cancer growth, progression and dissemination by Raman imaging, *Spectrochim. Acta - Part A Mol. Biomol. Spectrosc.* 198 (2018) 338–345, <https://doi.org/10.1016/j.saa.2018.02.058>.
- [41] B. Brozek-Pluska, M. Kopec, J. Surmacki, H. Abramczyk, Raman microspectroscopy of noncancerous and cancerous human breast tissues. Identification and phase transitions of linoleic and oleic acids by Raman low-temperature studies, *Analyst* 140 (2015) 2134–2143, <https://doi.org/10.1039/c4an01877j>.
- [42] R.R. Alfano, S.J. Wahl, A. Pradhan, G.C. Tang, Optical spectroscopic diagnosis of cancer and normal breast tissues, *J. Opt. Soc. Am. B* 6 (1989) 1015, <https://doi.org/10.1364/josab.6.001015>.
- [43] K. Kong, C. Kendall, N. Stone, I. Nottingher, Raman spectroscopy for medical diagnostics - From in-vitro biofluid assays to in-vivo cancer detection, *Adv. Drug Deliv. Rev.* 89 (2015) 121–134, <https://doi.org/10.1016/j.addr.2015.03.009>.

- [44] C. Kendall, M. Isabelle, F. Bazant-Hegemark, J. Hutchings, L. Orr, J. Babrah, R. Baker, N. Stone, Vibrational spectroscopy: A clinical tool for cancer diagnostics, *Analyst* 134 (2009) 1029–1045, <https://doi.org/10.1039/b822130h>.
- [45] D.T. Theodosis, D.A. Poulain, S.H.R. Oliet, Activity-dependent structural and functional plasticity of astrocyte-neuron interactions, *Physiol. Rev.* 88 (2008) 983–1008, <https://doi.org/10.1152/physrev.00036.2007>.
- [46] H. Abramczyk, A. Imiela, B. Brożek-Pluska, M. Kopeć, J. Surmacki, A. Śliwińska, Aberrant protein phosphorylation in cancer by using raman biomarkers, *Cancers (Basel)*, 11 (2019), <https://doi.org/10.3390/cancers11122017>.
- [47] J. Mill, T. Tang, Z. Kaminsky, T. Khare, S. Yazdanpanah, L. Bouchard, P. Jia, A. Assadzadeh, J. Flanagan, A. Schumacher, S.C. Wang, A. Petronis, Epigenomic Profiling Reveals DNA-Methylation Changes Associated with Major Psychosis, *Am. J. Hum. Genet.* 82 (2008) 696–711, <https://doi.org/10.1016/j.ajhg.2008.01.008>.
- [48] J.J. Miller, K.G. Baimbridge, Biochemical and immunohistochemical correlates of kindling-induced epilepsy: role of calcium binding protein, *Brain Res.* 278 (1983) 322–326, [https://doi.org/10.1016/0006-8993\(83\)90264-0](https://doi.org/10.1016/0006-8993(83)90264-0).
- [49] O. Uckermann, W. Yao, T.A. Juratli, R. Galli, E. Leipnitz, M. Meinhardt, E. Koch, G. Schackert, G. Steiner, M. Kirsch, IDH1 mutation in human glioma induces chemical alterations that are amenable to optical Raman spectroscopy, *J. Neurooncol.* 139 (2018) 261–268, <https://doi.org/10.1007/s11060-018-2883-8>.
- [50] B. Brozek-Pluska, M. Kopec, J. Surmacki, H. Abramczyk, Histochemical analysis of human breast tissue samples by IR and Raman spectroscopies. *Protocols discussion, Infrared Phys. Technol.* 93 (2018) 247–254, <https://doi.org/10.1016/j.infrared.2018.08.005>.
- [51] J. Surmacki, B. Brozek-Pluska, R. Kordek, H. Abramczyk, The lipid-reactive oxygen species phenotype of breast cancer. Raman spectroscopy and mapping, PCA and PLSDA for invasive ductal carcinoma and invasive lobular carcinoma. Molecular tumorigenic mechanisms beyond Warburg effect, *Analyst* 140 (2015) 2121–2133, <https://doi.org/10.1039/c4an01876a>.
- [52] H. Abramczyk, B. Brozek-Pluska, M. Kopec, J. Surmacki, M. Błaszczczyk, M. Radek, Redox Imbalance and Biochemical Changes in Cancer by probing redox-sensitive mitochondrial cytochromes in label-free visible resonance Raman imaging, *Cancers* 13 (2021) 1–20, <https://doi.org/10.3390/cancers13050960>.
- [53] M. Gasior-Głogowska, M. Komorowska, J. Hanuza, M. Maczka, M. Kobielarz, Structural alteration of collagen fibres - spectroscopic and mechanical studies, *Acta Bioeng. Biomech.* 12 (2010) 53–60.
- [54] H. Abramczyk, J. Surmacki, M. Kopeć, A.K. Olejnik, K. Lubecka-Pietruszewska, K. Fabianowska-Majewska, The role of lipid droplets and adipocytes in cancer. Raman imaging of cell cultures: MCF10A, MCF7, and MDA-MB-231 compared to adipocytes in cancerous human breast tissue, *Analyst* 140 (2015) 2224–2235, <https://doi.org/10.1039/C4AN01875C>.
- [55] H. Abramczyk, B. Brozek-Pluska, J. Surmacki, J. Jablonska-Gajewicz, R. Kordek, Raman “optical biopsy” of human breast cancer, *Prog. Biophys. Mol. Biol.* 108 (2012) 74–81, <https://doi.org/10.1016/j.pbiomolbio.2011.10.004>.